

Three-terminal perovskite/integrated back contact silicon tandem solar cells under low light intensity conditions

Kanda, Hiroyuki ; Dan Mihailetchi, Valentin ; Gueunier-Farret, Marie-Estelle ; Kleider, Jean-Paul ; Djebbour, Zakaria ; Alvarez, Jose ; Isabella, O.; Vogt, M.R.; Santbergen, R.; More Authors

DOI

[10.1002/idm2.12006](https://doi.org/10.1002/idm2.12006)

Publication date

2022

Document Version

Final published version

Published in

Interdisciplinary Materials

Citation (APA)

Kanda, H., Dan Mihailetchi, V., Gueunier-Farret, M.E., Kleider, J.P., Djebbour, Z., Alvarez, J., Isabella, O., Vogt, M. R., Santbergen, R., & More Authors (2022). Three-terminal perovskite/integrated back contact silicon tandem solar cells under low light intensity conditions. *Interdisciplinary Materials*, 1(1), 148-156. <https://doi.org/10.1002/idm2.12006>

Important note

To cite this publication, please use the final published version (if applicable).
Please check the document version above.



Copyright

Other than for strictly personal use, it is not permitted to download, forward or distribute the text or part of it, without the consent of the author(s) and/or copyright holder(s), unless the work is under an open content license such as Creative Commons.

Takedown policy

Please contact us and provide details if you believe this document breaches copyrights.
We will remove access to the work immediately and investigate your claim.

Three-terminal perovskite/integrated back contact silicon tandem solar cells under low light intensity conditions

Hiroyuki Kanda¹  | Valentin Dan Mihailetchi² |
 Marie-Estelle Gueunier-Farret^{3,4,5} | Jean-Paul Kleider^{3,4,5} |
 Zakaria Djebbour^{3,4,5} | Jose Alvarez^{3,4,5} | Baranek Philippe⁶ | Olindo Isabella⁷ |
 Malte R. Vogt⁷ | Rudi Santbergen⁷ | Philip Schulz⁵ | Fiala Peter⁸ |
 Mohammad K. Nazeeruddin¹ | James P. Connolly^{3,4} 

¹Group for Molecular Engineering of Functional Materials, École Polytechnique Fédérale de Lausanne, Valais Wallis, Sion, Switzerland

²International Solar Energy Research Center, ISC-Konstanz E.V., Konstanz, Germany

³CentraleSupélec, CNRS, Laboratoire de Génie Electrique et Electronique de Paris, Université Paris-Saclay, Gif-sur-Yvette, France

⁴CNRS, Laboratoire de Génie Electrique et Electronique de Paris, Sorbonne Unibversité, Paris, France

⁵CNRS, Institut Photovoltaïque d'Île de France (IPVF), Palaiseau, France

⁶Department EFESE, EDF Lab Paris-Saclay, EDF R&D, Palaiseau, France

⁷Delft University of Technology (TU Delft), Delft, The Netherlands

⁸Photovoltaics and Thin-Film Electronics Laboratory, Ecole Polytechnique Fédérale de Lausanne, Neuchâtel, Switzerland

Correspondence

Mohammad K. Nazeeruddin, Group for Molecular Engineering of Functional Materials, École Polytechnique Fédérale de Lausanne, Valais Wallis, Sion CH-1951, Switzerland.

Email: mdkhaja.nazeeruddin@epfl.ch

James P. Connolly, CNRS, Laboratoire de Génie Electrique et Electronique de Paris, Université Paris-Saclay, Centrale Supélec, Gif-sur-Yvette F-91192, France.

Email: James.Connolly@geeps.centralesupelec.fr

Funding information

H2020 program for Solar-ERANET funding of the BOBTANDEM (2019-2022)

Abstract

The current climate and energy crisis urgently needs solar cells with efficiencies above the 29% single junction efficiency bottleneck. Silicon/perovskite tandem solar cells are a solution, which is attracting much attention. While silicon/perovskite tandem cells in 2-terminal and 4-terminal configurations are well documented, the three-terminal concept is still in its infancy. It has significant advantages under low light intensities as opposed to concentrated sunlight, which is the critical factor in designing tandem solar cells for low-cost terrestrial applications. This study presents novel studies of the sub-cell performance of the first three-terminal perovskite/silicon selective band offset barrier tandem solar cells fabricated in an ongoing research project. This study focuses on short circuit current and operating voltages of the sub-cells under light intensities of one sun and below. Lifetime studies show that the perovskite bulk carrier lifetime is insensitive to illumination, while the silicon cell's lifetime decreases with decreasing light intensity. The combination of perovskite and silicon in the 3T perovskite-silicon tandem therefore reduces the sensitivity of V_{OC} to light intensity and maintains a relatively higher V_{OC} down to low light intensities, whereas silicon single-junction cells show a marked decrease. This technological advantage is proposed as a novel advantage

This is an open access article under the terms of the Creative Commons Attribution License, which permits use, distribution and reproduction in any medium, provided the original work is properly cited.

© 2022 The Authors. *Interdisciplinary Materials* published by Wuhan University of Technology and John Wiley & Sons Australia, Ltd.

of three-terminal perovskite/silicon solar cells for low light intensities of one sun or less.

KEYWORDS

low light intensity conditions, perovskite solar cells, tandem solar cells, three-terminal perovskite/Si solar cells

1 | INTRODUCTION

Tandem solar cells are currently the most promising route to achieving high conversion efficiency beyond single-junction solar cells.^[1] This study reports on the development of a novel device, the selective band offset three-terminal tandem that presents advantages over existing designs, which has been experimentally demonstrated by two groups.^[2,3]

The operation of tandem sub-cells as a function of incident light intensity reveals differences in operation rooted in materials and transport properties, which raise a number of promising research questions. In particular, the relative differences in performance as a function of the intensity of tandem structures relative to single-junction cells shows great potential for applications under lower light intensity.^[4] There is, therefore, great interest in analyzing the relative performance of tandem sub-cells as a function of incident light intensity, to evaluate the advantages of these structures under one sun and, by inference, to lower light intensities.

The materials system studied is the tandem solar cell architecture consisting of a perovskite sub-cell as a higher bandgap top cell, and a silicon sub-cell as a lower bandgap bottom cell.^[5–12] This material system is currently the object of major global research efforts aimed at achieving high conversion efficiency compatible with the dominant silicon solar cell technologies. The tandem solar cell theoretical limiting efficiency context of, maximum photoconversion efficiency is 45.1% for the 2-terminal, 45.3% for the three-terminal (3T), and 44.5% for the four-terminal (4T) tandem solar cells according to the Shockley–Queisser limit.^[13,14] By considering practical limits including real material limitations, a potential photoconversion efficiency of up to 35% is projected for perovskite/silicon tandem solar cells.^[15]

This study considers a novel 3T device architecture, which features a carrier selective band offset barrier,^[3] delivering 3T tandem efficiencies without the need for lateral transport layers, which contribute to parasitic absorption losses. In addition, the design eliminates the need for grid alignment to minimize shading that is a constraint in 4T designs. Finally, the broader ideal efficiency contour of the 3T device further allows greater flexibility in the top

and bottom cell bandgaps. Therefore, the choice of materials in this 3T perovskite/silicon tandem solar cell introduces an important advantage, which is the availability of perovskite bandgaps in the wide range of 1.4–2.2 eV. For these materials, the silicon/perovskite tandem radiative limit can reach 42% efficiency under one sun.^[2]

We now consider the performance of silicon and perovskite materials in a tandem solar cell as a function of light intensity, and the variation of cell performance as a function of carrier lifetime, in particular considering the open-circuit voltage. At low light intensity, the short-circuit current density varies linearly with light intensity. Notably, the open-circuit voltage of each sub-cell, operating independently in the 3T configuration, is described by Equation (1) for Shockley diode recombination currents in the classic light and dark current superposition picture

$$V_{OC} \approx \frac{KT}{e} \ln \frac{J_{SC}}{J_0}, \quad (1)$$

where K is Boltzman's constant, T the temperature, J_{SC} the short circuit current, e the electronic charge, and J_0 the saturation dark current. We note that under low light conditions V_{OC} will decrease logarithmically with decreasing short-circuit current (Equation 1). We can evaluate the sensitivity to the carrier lifetime by considering the saturation dark current of each sub-cell, which is given by the classic diode equation in case of an abrupt p^+n junction^[16] as follows:

$$J_0 \approx q \sqrt{\frac{D_p}{\tau_p}} \frac{n_i^2}{N_D}, \quad (2)$$

where D_p is the diffusion constant of holes, τ_p is the minority carrier lifetime, n_i is the intrinsic carrier concentration, N_D is the donor concentration. In contrast to the dependence on J_{SC} , we see from Equation (2) that decreasing carrier lifetime τ will lead to the square of the inverse of the lifetime and therefore proportionately stronger increase in the dark current saturation.

A decrease of minority carrier lifetime with decreasing light intensity will therefore lead to a superlinear decrease of J_{SC}/J_0 , thus amplifying the decrease in V_{OC} compared to the simple logarithmic decrease expected

from the dependence on short-circuit current only. This is the case in Si, where carrier lifetime is severely decreased with decreasing light intensity, resulting in V_{OC} changes by varying the light illumination.^[17,18]

In contrast, the carrier lifetime of perovskite is not sensitive to light intensity, and therefore the perovskite solar cell V_{OC} is therefore much more robust against lowering of light intensity.^[19]

This yields an important advantage of the 3T perovskite/silicon tandem solar cells, which is that it can maintain the high V_{OC} at low light intensity due to the perovskite characteristics reducing sensitivity to low light intensity.

In this study, we have therefore investigated photovoltaic characteristics under low light intensity for 3T perovskite/silicon tandem solar cells. The tandem solar cells were characterized for the photovoltaic performances under one sun illumination and the carrier dynamics of perovskite and silicon semiconductor evaluated.

To achieve this, the photovoltaic properties of the tandem solar cells were measured by changing the light intensity in the range from one sun to a fraction of sun, that is, from 100 to 1.5 mW cm⁻² irradiation.

The resulting cell performance parameters are compared for both the perovskite top solar cells and the silicon bottom solar cells. Moreover, carrier dynamics of the perovskite and silicon semiconductor were characterized for an in-depth understanding of the V_{OC} changes under low light illumination by using time-resolved photoluminescence spectroscopy together with a Shockley-Read-Hall (SRH) recombination model.

The shortcomings of parasitic absorption of internal TCO layer in 4-terminal perovskite/silicon tandem solar cell and bandgap tuning of perovskite to get current matching in a 2-terminal tandem cell can be overcome by using the 3T perovskite/silicon tandem solar cells.

The 3T tandem solar cell, while a promising device due to the technical advantages we have seen, furthermore shows advantages as specified in this study under low light intensity conditions, which is beneficial to an independent power supply.

2 | EXPERIMENTAL DETAILS

We demonstrate the photovoltaic performance under low light intensity for novel 3T perovskite/silicon tandem solar cells by changing the irradiation. Figure 1 shows a schematic of the device structure and cross-sectional scanning electron microscope (SEM) image of the 3T tandem solar cell. The top cell consists of n-i-p configuration involving SnO_x, triple-cation perovskite, poly[bis(4-phenyl)(2,4,6-trimethylphenyl)amine] (PTAA), MoO_x, indium zinc oxide layer, and Au grid layer. The SnO_x is the electron transport layer (ETL), which due to electron affinity matching shows little or no band discontinuity in the conduction band. This allows electrons to flow unimpeded from the perovskite cell to the silicon cell, that is, allows the photocurrent flow in the opposite direction, from the silicon bottom cell to the perovskite top cell side (Figure 1A,B).

However, because of the larger forbidden bandgap of SnO_x, relative to Si and to the perovskite, there is a large barrier in the valence band, and hole transport from the perovskite solar cell (PSC) to the interdigitated back contact cell (IBC) is blocked. Therefore, holes in the perovskite cannot thermalize to the silicon bottom cell. This decouples the hole populations in the top and bottom cells, and produces different quasi-Fermi level separations in the top and bottom cells, and decouples their operation as a function of applied voltage, yielding independent operation, and allowing the device to reach tandem solar cell efficiencies.

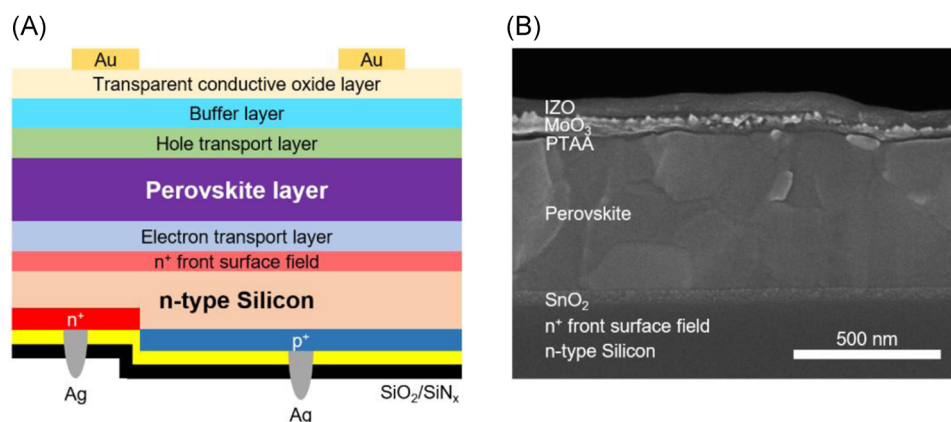


FIGURE 1 Schematics image of (A) three-terminal perovskite silicon tandem solar cells and (B) cross-sectional scanning electron microscope image of PSC top cell on interdigitated back contact

The triple-cation perovskite layer was chosen as a photo absorber for the top cell at short wavelengths. The perovskite bandgap is 1.54 eV, which is an acceptable value since the 3T perovskite/silicon tandem configuration has a wide tolerance margin for the bandgap (1.4–2.2 eV) due to the broad bandgap-radiative efficiency maximum of this design.^[2] PTAA is chosen as the hole transport layer (HTL), which extracts holes from the perovskite to the top front electrode. MoO_x is selected as a buffer layer to protect the HTL from the sputtering damage resulting from the deposition of the transparent conductive oxide layer (TCO).^[20] The indium zinc oxide layer is the TCO layer conducting the current to the front electrode Au grid. The bottom silicon absorber used to absorb the long wavelength light is an IBC silicon solar cell. The IBC silicon solar cells are composed of an n-type silicon substrate with heavily doped p⁺ and n⁺ layers as anode and cathode, respectively, which constitute the IBCs. An n⁺ front surface layer is provided on the n-type silicon surface. The SiO₂/SiN_x layer stack plays a role as a passivation layer to reduce the recombination velocity of the silicon rear surface. An Ag integrated grid contacts the p⁺ and n⁺ layers, respectively.

A noteworthy point is that there are two different circuits for current flow. The current flow (a) is n⁺→n-type silicon→n⁺ front surface field→ETL→perovskite→HTL→front electrode, the other current flow (b) is n⁺→n-type silicon→p⁺. The current flows of (a) and (b) are photogenerated by the perovskite top cell and the silicon bottom cell, respectively.

3 | RESULTS AND DISCUSSION

The photovoltaic properties of the 3T perovskite/silicon tandem solar cell (100 mW cm⁻²) are shown in Figure 2. Note that the perovskite top cell current-voltage curve

was measured while holding the bottom cell voltage fixed at its maximum power point, and vice versa.

Figure 2A shows the current-voltage characteristics of perovskite and silicon sub-cells. We note that the perovskite cell features a poor fill factor, which is due to the fact that this is the first embodiment of the full 3T structure fabricated within the BOBTandem European Solar-ERA. NET research project.^[21] The optimization of the structure is the subject of active development, which is however beyond the scope of this study, which focuses on sub-cell short circuit currents and operating voltages as a function of light intensity. We only note that the low fill factor is primarily due to a preliminary prototype perovskite solar cell, which has not been optimized. The energy level diagram is shown in Figure S1. The electron affinity matching of SnO_x shows no band discontinuity in the conduction band through the silicon to the perovskite layer. Therefore, electrons flow smoothly from the perovskite top cell to the silicon bottom cell, enabling them to yield the power as 3T-tandem solar cells.

The J_{SC} of the perovskite and silicon solar cells are 13.1 and 11.4 mA cm⁻², respectively. The silicon sub-cell J_{SC} is diminished compared to a single-junction silicon solar cell J_{SC} because of the perovskite sub-cell absorption, which only transmits radiation of a wavelength longer than 800 nm to the silicon sub-cell. The V_{OC} of the perovskite and silicon cells are 930 and 550 mV, respectively. The fill factor (FF) of the perovskite top cell is 0.504, which is significantly lower than reported for perovskite solar cells for these early and un-optimized devices, for which the TCO layer conductivity is the main cause as mentioned previously. As a result, the photoconversion efficiency achieved is 5.4% for the perovskite top cell, 4.8% for the silicon bottom cell, and 10.2% (=5.4% + 4.8%) for the overall 3T perovskite silicon tandem solar cell. Figure 2B shows incident photon-to-current efficiency (IPCE) for perovskite top (blue line) and silicon bottom (red line)

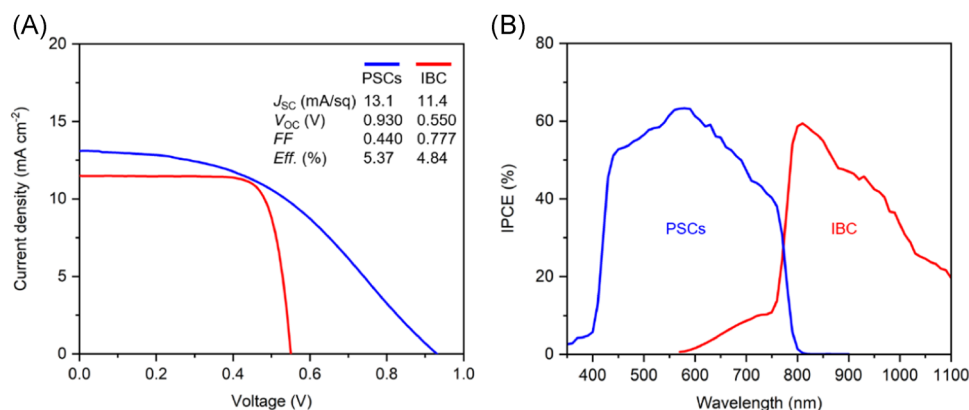


FIGURE 2 (A) Photovoltaic properties and IV curves of PSC top and interdigitated back contact (IBC) bottom cells and that of (B) incident photon-to-current efficiency

solar cells. We investigated how the applied bias voltage on the bottom cell affects the results for the top cell. The photovoltaic parameter of the top cell as a function of the applied bias on the bottom cell are shown in supplemental Table S1. The bias voltage of the bottom cell was applied at 0 and 0.48 V (maximum-power point voltage of bottom cell). The photoconversion efficiency difference between 0 and 0.48 V was 0.07%, which indicates that applied bias voltage on the bottom cell does not significantly affect the result of the top cell. This means that the two current flow pathway seems not to interfere with each other, thus the top and the bottom cells can output power independently.

To investigate the photovoltaic performance of 3T perovskite/silicon tandem solar cells at a low light intensity, we measured *IV* curves and plotted the normalized photovoltaic properties as a function of the light intensity in the range of 1.5–100 mW cm^{-2} as shown in Figure 3. The device performance of PSCs and IBC are shown in Figure S2 and Table S2. The normalized J_{SC} values were changed linearly by changing the light intensity for the perovskite top and silicon bottom solar cells (Figure 3A).

We first note that the normalized V_{OC} of the perovskite top cell (red dots, Figure 3B) shows a weak and quasi-linear dependence on incident spectrum intensity from 100 to 1.5 mW cm^{-2} , the relative decrease being only 12%.

In contrast, the V_{OC} of the silicon bottom solar cell (blue dots, Figure 3B) decreases much more significantly over the same intensity range, with a relative decrease of over 80% (Figure 3B). This observation is consistent with a perovskite carrier lifetime remaining relatively constant, while the carrier lifetime of the silicon cell decreases strongly with decreasing light intensity.

We next note that the V_{OC} variation with light intensity in the 3T tandem structure is the sum of the V_{OC} of top and bottom sub-cells and that this overall 3T tandem is less sensitive to the decrease of silicon cell V_{OC} with decreasing light intensity. This analysis therefore concludes that overall the 3T perovskite/silicon tandem solar cells maintain a higher V_{OC} under the low light intensity, compared to the relative drop of a single junction silicon solar cell, due to the relatively weak intensity dependence of the perovskite sub-cell open-circuit voltage. Noteworthy, 3T perovskite/silicon tandem solar cells represent reduced sensitivity of the V_{oc} to light intensity compared with single-junction cells. For instance, silicon bottom cell of 3T tandem decreased the V_{oc} from 0.565 V (100 mW cm^{-2}) to 0.081 V at 1.5 mW cm^{-2} , while single-junction silicon solar cells can maintain around 500 mV (1.5 mW cm^{-2}) owing to the front surface passivation layer (e.g., SiN_x).^[22] Regarding the perovskite top cells, the V_{oc} sensitivity is lower than the single-junction perovskite solar cells.

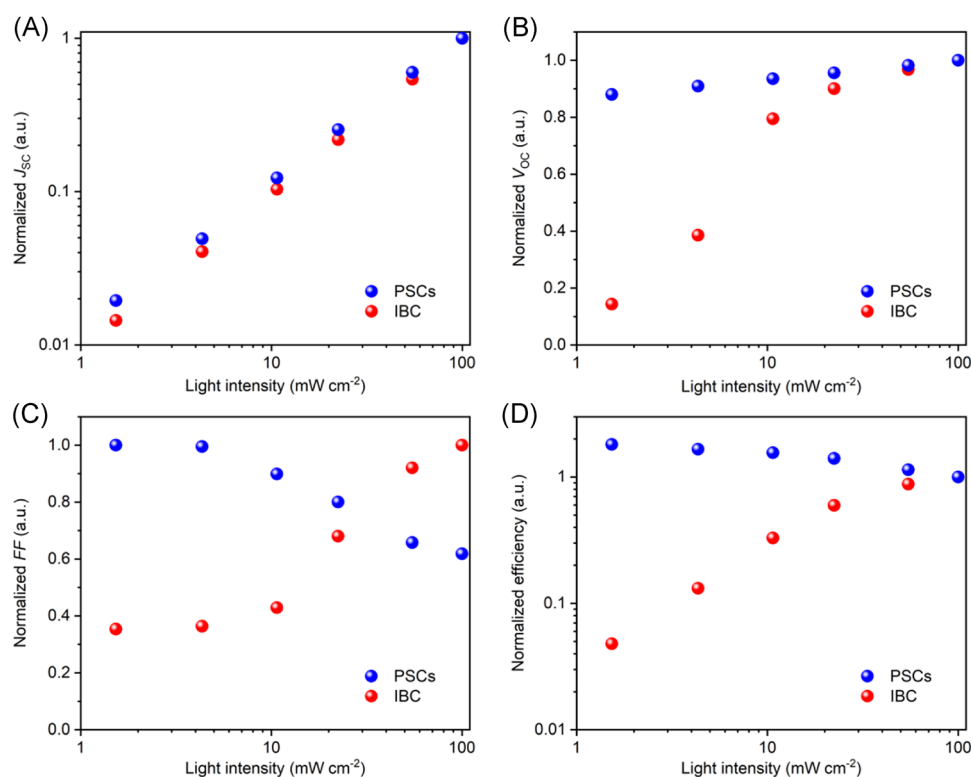


FIGURE 3 Photovoltaic performances as a function of light intensity of (A) J_{SC} , (B) V_{OC} , (C) FF , and (D) photoconversion efficiency for PSC top and interdigitated back contact (IBC) bottom cells. Each plot is normalized to the highest value

This might be due to the reduced ideal diode factor by the TCO sputtering damage on the HTL.^[20] These defect passivation/suppression for perovskite top cells and silicon bottom cells are the key to increasing the V_{OC} sensitivity to light intensity beyond the current state of the art. Concerning the normalized FF , and despite the low FF values for questions of device optimization mentioned earlier, the results show the well-known phenomenon of a tandem solar cell of the reduced short-circuit current, relative to a single junction solar cell helping to maintain FF . This is due to decreased sensitivity to series resistance resulting from the reduced sub-cell short current densities (Figure 3C). On the other hand, the FF of the silicon solar cell was decreased to 38% at the 1.5 mW cm^{-2} . This reason can be related to carrier recombination as discussed below. As a consequence, the normalized conversion efficiency of the perovskite top cells is maintained at the lower light intensity in the range studied, while the silicon bottom cells photoconversion efficiency decreases due to the V_{OC} and FF drop (Figure 3D).

For further investigation of the reason behind the V_{OC} changes, we performed Suns- V_{OC} measurements^[23] yielding ideality factors for the two sub-cells and carrier lifetime characterization, as shown in Figure 4. In Figure 4A, Suns- V_{OC} plot PSCs are linear in the range of the $1.5\text{--}100 \text{ mW cm}^{-2}$ while the tendency of the IBC is changed between $1.5\text{--}10.7 \text{ mW cm}^{-2}$ and $10.7\text{--}100 \text{ mW cm}^{-2}$. This indicates that the PSCs can adequately be described with a single diode model since the PSC pseudo-dark current Suns- V_{OC} plot is linear. The IBC, on the other hand, showing two linear regimes, must be described with a two diode model. This is consistent with Reich et al.'s work on V_{OC} behavior under the low light intensity analyzed with a double-diode model.^[24]

We applied an equivalent circuit model of the 3T tandem solar cells as shown in Figure 4B. Fitting parameters are shown in supplemental Table S3. The obtained ideality factor of PSC top solar cell (n_{PSC}) was 1.6, while the ideality factor of n_{IBC_a} and n_{IBC_b} for IBC were 1.38 and 6.0, respectively. This high ideality factor of n_{IBC_b} suggests that carrier recombination in the silicon bottom solar cells at low intensities becomes dominated by other mechanisms, such as edge recombination and front surface recombination.

We have characterized carrier lifetime (τ) as a function of the photogenerated carrier density to understand the V_{OC} transition of perovskite top and silicon bottom solar cells (Figure 4B). We measured the carrier lifetime of the perovskite layer by time-resolved photoluminescence spectroscopy while varying the photogenerated carrier density. The sample was prepared as a perovskite/glass structure to eliminate the effect of the HTL and ETL layers. The thickness of the perovskite layer is the same as the 3T device architecture. Measured spectra were fitted by single-exponential decay and obtained carrier lifetimes ($\tau_{\text{perovskite}}$) were normalized to the value at $1 \times 10^{15} \text{ cm}^{-3}$ excess carrier density. Measured spectra and calculated values were shown in Figure S3 and Table S4, respectively. Notably, the normalized $\tau_{\text{perovskite}}$ was not changed strongly by decreasing the photogenerated carrier density. This result is consistent with the Suns- V_{OC} (Figure 4A) and high V_{OC} at the low light intensity (Figure 3B). Regarding the silicon, the carrier lifetime can be decreased by the edge recombination and the front surface recombination due to the absence of passivation layers in these prototype devices, which causes the V_{OC} drop at low light intensity. We also note that the injection-carrier-dependent bulk lifetime plays a part in the V_{OC} drop. The lifetime was according to

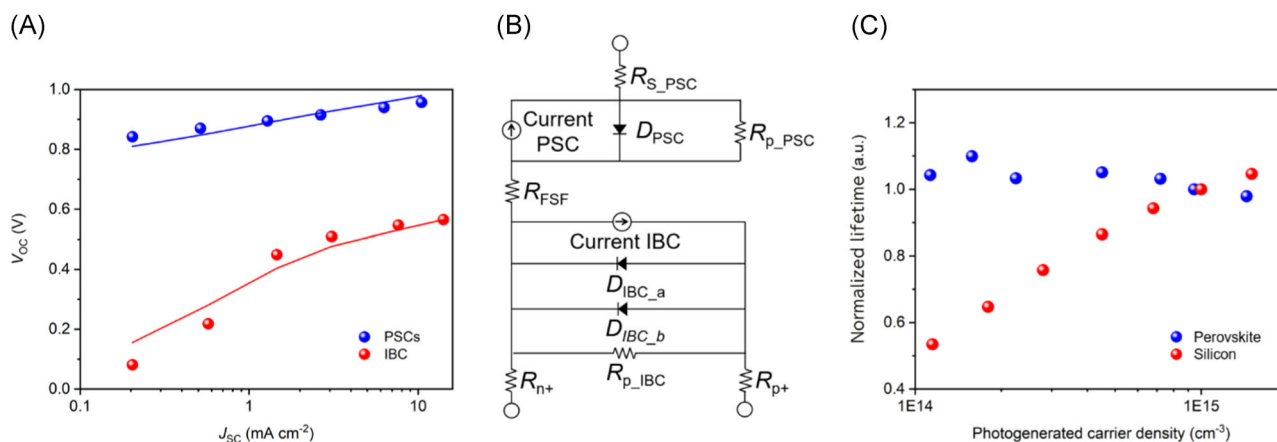


FIGURE 4 (A) Suns V_{OC} plot for PSC top and interdigitated back contact bottom cells, where lines are guides to the eye showing a moderate decrease in V_{OC} for the perovskite cell and a stronger dependence at low light intensity for the Si cell. Blue and red lines are the fitting lines. (B) equivalent circuit model for three-terminal tandem solar cells. (C) Carrier lifetime as a function of photogenerated carrier density of perovskite and silicon. Carrier lifetime was obtained by time-resolved photoluminescence decay and Shockley-Read-Hall model for perovskite and silicon, respectively

an SRH model,^[25,26] such that lifetimes τ_{n0} and τ_{p0} are evaluated as follows

$$\tau_{n0} = \frac{1}{N\sigma_n v_{th}}, \quad (3)$$

$$\tau_{p0} = \frac{1}{N\sigma_p v_{th}}, \quad (4)$$

where N is recombination center density, σ_n and σ_p are capture cross-sections, v_{th} is the thermal velocity, taken identical for electrons and holes. In this nondegenerate perovskite material, the equilibrium concentrations of electrons and holes are described in the standard Boltzmann approximation as follows:

$$n_1 = N_C \exp\left(\frac{E_T - E_C}{kT}\right), \quad (5)$$

$$p_1 = N_V \exp\left(\frac{E_C - E_G - E_T}{kT}\right), \quad (6)$$

where N_C and N_V are densities states at the conduction and valence band edge for the silicon, respectively. E_T , E_C , and E_G are energy of the recombination center, conduction band edge, and energy band gap, respectively. Then, SHR lifetime (τ_{SRH}) as a function of the excess carrier density Δn is then given by

$$\tau_{SRH} = \frac{\tau_{p0}(n_0 + n_1 + \Delta n) + \tau_{n0}(p_0 + p_1 + \Delta p)}{n_0 + p_0 + \Delta n}, \quad (7)$$

assuming $\Delta n = \Delta p$. The estimated carrier lifetime of the silicon ($\tau_{silicon}$) as a function of the photogenerated carrier density was normalized at the $1 \times 10^{15} \text{ cm}^{-3}$ value. The normalized $\tau_{silicon}$ was decreased according to the decreasing photogenerated carrier density (Figure 4B). The V_{OC} trend is consistent with that reported in the literature.^[27] Consequently, we conclude that the V_{OC} trend is related to the variation of carrier lifetime as a function of the photogenerated carrier density of the perovskite and silicon semiconductor. For these reasons, perovskite top cells can feature a high V_{OC} under low ($1.5\text{--}10.7 \text{ mW cm}^{-2}$) and high-intensity conditions ($10.7\text{--}100 \text{ mW cm}^{-2}$), while silicon bottom cells can yield high V_{OC} at high light intensity irradiation ($10.7\text{--}100 \text{ mW cm}^{-2}$).

These analyses demonstrate that the 3T perovskite/silicon tandem solar cells feature a V_{OC} , which is maintained due to the relatively weak variation of the perovskite top cell V_{OC} across the range of low light intensities studied, while under high light intensity, both top and bottom cell operate at higher V_{OC} consistent with their respective carrier lifetime properties at the higher light intensity. In

other words, due to the action of the perovskite top sub-cell reducing V_{OC} degradation at low intensities, the 3T perovskite/silicon tandem solar cells can find applications not only under 100 mW cm^{-2} illumination but also under lower light intensity conditions ($<10 \text{ mW cm}^{-2}$) as demonstrated experimentally.

4 | CONCLUSIONS

In conclusion, we have demonstrated the photovoltaic performance of 3T perovskite/silicon solar cells under light intensity conditions of one sun and below. Device performance at low light intensities was analyzed in terms of carrier lifetimes of perovskite and silicon semiconductors. The perovskite top cell maintains high V_{OC} under the lower light intensity, whereas the V_{OC} of the silicon bottom cell shows a stronger than expected decrease with decreasing light intensity below $\sim 10 \text{ mW/cm}^2$ (i.e., <0.1 sun). The carrier lifetime of the perovskite sub-cell is maintained as light intensity is decreased, whereas the carrier lifetime of the silicon sub-cell decreases strongly over the same conditions. Three-terminal perovskite/silicon tandem solar cells can therefore maintain high V_{OC} from perovskite top cells under low light illumination, by moderating the impact on the 3T operation from the decreased Si solar cell V_{OC} at low light intensities. Consequently, we show that the 3T perovskite/silicon tandem solar cells achieve two things. The first is to increase Si cell solar efficiencies in a tandem configuration without current or optical matching constraints with important technological device design advantages due to the reduced constraints. The second is that the 3T tandem device could work efficiently not only under 100 mW cm^{-2} but also under the low light intensity condition, because the device is less sensitive to the V_{OC} decrease in the Si solar cell. This second point is beneficial to an independent power supply under low light conditions. Following this demonstration of the 3T-SBOB concept and investigation of its performance as a function of light intensity, the next steps will be to optimize cell design to reach efficiencies over 30% under one sun.

5 | EXPERIMENTAL

5.1 | Materials

To fabricate the perovskite layer, methylammonium bromide, and formamidinium iodide were purchased from GreatCell Solar Ltd. Lead iodide and lead bromide was purchased from TCI Co. Ltd. Cesium iodide was obtained from ABCR GmbH. Tin oxide dispersed solution was purchased from Alfa Aesar. Bis(trifluoromethane)sulfonimide lithium salt was purchased from Sigma-Aldrich. All of the

purchased chemicals were used as received without further purification.

5.2 | Device fabrication and measurement

For the perovskite top cells, UV/O₃ cleaning of the IBC silicon substrate was performed, following which a tin oxide (SnO_x) layer was deposited on the IBC silicon substrate by spin-coating process (4000 rpm for 30 s) with SnO_x nanoparticles dispersed solution (7.5% in water) then dried at 125°C for 5 min. After UV/O₃ treatment for 30 min, a perovskite layer was formed on the SnO_x layer. The perovskite solution was 1.3M (CsPbI₃)_{0.1}(FAPbI₃)_{0.875}(MAPbBr₃)_{0.125} dissolved in DMF:DMSO = 4:1 (volume ratio).^[28] The perovskite solution was spin-coated on the SnO₂ layer (two-step program: 1000 rpm for 10 s and 5000 rpm for 30 s).^[29] An anti-solvent of chlorobenzene was dropped onto the film surface 10 s before finishing the spin-coating recipe, followed by annealing the samples at 100°C for 1 h to form the perovskite layer. Subsequently, poly[bis(4-phenyl)(2,4,6-trimethylphenyl)amine] (PTAA) as a hole-transport layer was formed on the perovskite layer by spin-coating (4000 rpm, 30 s). The HTL solution was prepared by dissolving 10 mg of PTAA (Emindex) with additives in 1 ml of toluene. As additives, 7.5 μl of Bis(trifluoromethane)sulfonimide lithium salt (Aldrich) from the stock solution (170 mg in 1 ml of acetonitrile), and 4 μl of 4-*tert*-butylpyridine were added. Thereby, 10 nm of MoO_x layer by evaporation, 100 nm of indium zinc oxide (IZO) layer by sputtering, and gold grid contact by evaporation were deposited.

The IBC cell concept used in this study is based on ISC-Konstanz's ZEBRA cell technology that is currently in mass production with an average conversion efficiency exceeding 23.5%.^[22] The IBC cells were fabricated on M2 (156.75 mm) n-type Cz wafers with a resistivity range of 4–7 Ωcm and a thickness of 170 ± 10 μm. The fabrication process sequence of IBC cells for tandem integration follows that used in mass production,^[22] with only minor process adaptations. It uses high-temperature Boron and Phosphorous diffusions to form the 150 ± 15 Ω/sq p⁺ and n⁺ doped regions, thermal SiO₂ and PECVD SiNx deposition for surface passivation stack, as well as screen printing and firing-through metallization steps. The only process adaptations required for the tandem integration were to realize a flat chemically etched front side without an antireflection coating layer to facilitate the spin-coating processes for the top cell layers.

Since all process steps to fabricate these IBC cells require a high temperature of more than 450°C, the IBC

bottom cells were completely fabricated, including electrical contacts, before the perovskite top cell processing. On each M2 n-type wafer, 100 mini IBC cells with an area of 14.3 × 14.3 mm² were fabricated and subsequently separated, by means of layer scribing, before top cell integration.

IV measurements were made using an Oriel VeraSol solar simulator (Newport Corporation) by using calibrator LCE-50 (Centronics). The IV measurement was performed from 1 to 0 V as a reverse scan, with a mask of 0.13 cm² for perovskite, and 1 cm² for silicon bottom cells. The scanning step and speed were 10 mV and 50 mV/s, respectively. Time-resolved photoluminescence spectroscopy was performed by Fluorolog TCSPC with an excitation wavelength of 640 nm (HORIBA, Ltd.) with an ND filter. Morphology was measured by cold field emission SEM (SU8200, Hitachi high-tech. Co.).

ACKNOWLEDGMENTS

The authors acknowledge the support of the H2020 program for Solar-ERANET funding of the BOBTANDEM (2019–2022).

CONFLICT OF INTERESTS


The authors declare that there are no conflict of interests.

AUTHOR CONTRIBUTIONS

Hiroyuki Kanda fabricated PSC devices, characterized for IV, SEM, PL measurement, and wrote the manuscript. Valentin Dan Mihailitchi and Fiala Peter fabricated IBC bottom solar cells and the top electrode layer, respectively. James P. Connolly is coordinating the BOBTANDEM project. All authors contributed to discussions and to finalizing the manuscript.

ORCID

Hiroyuki Kanda  <http://orcid.org/0000-0002-0327-8775>

James P. Connolly  <https://orcid.org/0000-0003-0342-1719>

REFERENCES

- [1] De Vos A. Detailed balance limit of the efficiency of tandem solar cells. *J Phys D Appl Phys*. 1980;13:839-846.
- [2] Connolly JP, Ahanobge K, Kleider J-P, et al. Recent results on carrier selective three terminal perovskite on silicon-IBC tandem solar cells, *37th edition of the european photovoltaic solar energy conference and exhibition (EU PVSEC)*; 2020.
- [3] Djebbour Z, El-Huni W, Migan Dubois A, Kleider J. Bandgap engineered smart three-terminal solar cell: new perspectives towards very high efficiencies in the silicon world. *Prog Photovoltaics Res Appl*. 2019;27:306-315.
- [4] Yamamoto K, Okada K, Nakayama M, et al. Chronic subdural hematoma infected by propionibacterium acnes: a case report. *Fujikura Tech Rev*. 2015;45:6-14.

- [5] Bush KA, Palmstrom AF, Yu ZJ, et al. 23.6%-efficient monolithic perovskite/silicon tandem solar cells with improved stability. *Nat Energy*. 2017;2:17009.
- [6] McMeekin DP, Sadoughi G, Rehman W, et al. A mixed-cation lead mixed-halide perovskite absorber for tandem solar cells. *Science*. 2016;351:151-155.
- [7] Kanda H, Shibayama N, Uzum A, et al. Effect of silicon surface for perovskite/silicon tandem solar cells: flat or textured? *ACS Appl Mater Interfaces*. 2018;10:35016-35024.
- [8] De Bastiani M, Mirabelli AJ, Hou Y, et al. Efficient bifacial monolithic perovskite/silicon tandem solar cells via bandgap engineering. *Nat Energy*. 2021;6:167-175.
- [9] Werner J, Weng CH, Walter A, et al. Efficient monolithic perovskite/silicon tandem solar cell with cell area >1 cm². *J Phys Chem Lett*. 2016;7:161-166.
- [10] Al-Ashouri A, Köhnen E, Li B, et al. Monolithic perovskite/silicon tandem solar cell with >29% efficiency by enhanced hole extraction. *Science*. 2020;370:1300-1309.
- [11] Albrecht S, Saliba M, Correa Baena JP, et al. Monolithic perovskite/silicon-heterojunction tandem solar cells processed at low temperature. *Energy Environ Sci*. 2016;9:81-88.
- [12] Chen B, Zheng X, Bai Y, Padture NP, Huang J. Progress in tandem solar cells based on hybrid organic-inorganic perovskites. *Adv Energy Mater*. 2017;7:1602400.
- [13] Shockley W, Queisser HJ. Detailed balance limit of efficiency of p-n junction solar cells. *J Appl Phys*. 1961;32:510-519.
- [14] Tockhorn P, Wagner P, Kegelmann L, et al. Three-terminal perovskite/silicon tandem solar cells with top and interdigitated rear contacts. *ACS Appl Energy Mater*. 2020;3:1381-1392.
- [15] Schneider BW, Lal NN, Baker-Finch S, White TP. Pyramidal surface textures for light trapping and antireflection in perovskite-on-silicon tandem solar cells. *Opt Express*. 2014;22:A1422-A1430.
- [16] Sze SM, Ng KK. *Physics of semiconductor devices*. John Wiley & Sons, Inc; 2006.
- [17] Hieslmair H, Appel J, Kasthuri J, Guo J, Johnson B, Binns J. Impact of the injection-level-dependent lifetime on Voc, FF, ideality, J02, and the dim light response in a commercial PERC cell: impact of the injection-level-dependent lifetime. *Prog Photovoltaics Res Appl*. 2016;24:1448-1457.
- [18] Chen D, Kim M, Shi J, et al. Progress in photovoltaics: research and applications. 2019; pip. 3230.
- [19] Raifuku I, Ishikawa Y, Ito S, Uraoka Y. Characteristics of perovskite solar cells under low-illuminance conditions. *J Phys Chem C*. 2016;120:18986-18990.
- [20] Kanda H, Uzum A, Baranwal AK, et al. Analysis of sputtering damage on I-V Curves for perovskite solar cells and simulation with reversed diode model. *J Phys Chem C*. 2016;120:28441-28447.
- [21] H2020 (Solar-ERANET) project BOBTANDEM. <https://bobtandem.wordpress.com/Twitter>; <https://twitter.com/bobtandem>
- [22] Kopecek R, Libal J, Lossen J, et al. 2020 47th IEEE Photovoltaic Specialists Conference, IEEE, 2020; pp. 1008-1012.
- [23] Shibayama N, Kanda H, Kim TW, Segawa H, Ito S. Design of BCP buffer layer for inverted perovskite solar cells using ideal factor. *APL Mater*. 2019;7:031117.
- [24] Reich NH, Sark WJHMV, Alsema EA, et al. Crystalline silicon cell performance at low light intensities. *Sol Energy Mater Sol Cells*. 2009;93:1471-1481.
- [25] Shockley W, Read WT. Statistics of the recombinations of holes and electrons. *Phys Rev*. 1952;87:835-842.
- [26] Macdonald D, Cuevas A. Validity of simplified shockley-read-hall statistics for modeling carrier lifetimes in crystalline silicon. *Phys Rev B Condens Matter Mater Phys*. 2003;67:075203.
- [27] Kanda H, Shibayama N, Uzum A, et al. Facile fabrication method of small-sized crystal silicon solar cells for ubiquitous applications and tandem device with perovskite solar cells. *Mater Today Energy*. 2018;7:190-198.
- [28] Li W, Cui J, Zheng D, et al. Fabrication and characteristics of heavily Fe-doped LiNbO₃/Si Heterojunction. *Materials (Basel)*. 2019;12:2659.
- [29] Abuhelaiqa M, Shibayama N, Gao X-X, Kanda H, Nazeeruddin MK. *ACS Appl Energy Mater*. 2021; acaem.0c03185.

SUPPORTING INFORMATION

Additional supporting information may be found in the online version of the article at the publisher's website.

How to cite this article: Kanda H, Dan Mihailetchi V, Gueunier-Farret M-E, et al. Three-terminal perovskite/integrated back contact silicon tandem solar cells under low light intensity conditions. *Interdiscip Mater*. 2022;1:148-156. doi:10.1002/idm2.12006